Non-uniform hydrogen attack cavitation and the role of interaction with creep

van der Burg, M.W.D.; van der Giessen, E.

Published in:
Materials science and engineering a-Structural materials properties microstructure and processing

DOI:
10.1016/S0921-5093(96)10465-2

Publication date:
1996

ELSEVIER

Materials Science and Engineering A220 (1996) 200–214

MATERIALS SCIENCE & ENGINEERING A

Non-uniform hydrogen attack cavitation and the role of interaction with creep

M.W.D. van der Burg, E. van der Giessen*

Delft University of Technology, Laboratory for Engineering Mechanics, 2628 CD Delft, The Netherlands

Received 28 February 1996; revised 1 July 1996

Abstract

Hydrogen attack (HA) is the development of grain-boundary porosity by cavities filled with high-pressure methane that originates from the reaction of carbides with hydrogen at high temperatures. The cavities grow by grain-boundary diffusion and by creep of the adjacent grain material till they coalesce with neighbouring cavities to form a microcrack. Earlier work on HA has focussed on unit cells containing a single cavity, using average cavitation properties. Here, non-uniform cavitation properties on the grain-size scale are assumed in a polycrystalline aggregate, and unit cell analyses are performed to investigate the influence of the adjacent grains on the development of the grain-boundary HA. The numerical results are explained in terms of two simplified models which highlight the key parameters governing the grain deformation–grain boundary cavitation interaction process.

Keywords: Hydrogen attack; Cavitation; Creep

1. Introduction

Hydrogen attack (HA) is a well-known low-ductility type of failure in steels exposed to high-pressure hydrogen at elevated temperatures as is relevant in, for example, petrochemical applications [1]. A failure due to HA can be recognized by intergranular fracture, which is initiated by porous damage of the grain-boundary facet. This damage develops as a result of the fact that at these elevated temperatures, hydrogen can diffuse into the steel, where a chemical reaction takes place with the carbides. Due to this reaction, a cavity is formed that is filled by methane gas, which is trapped in the material. Depending on the stability of the carbide, the equilibrium methane pressure can be of the order of the ambient hydrogen pressure, or two orders of magnitude higher (see [2]). Together with any applied stresses from the loading of the component, the internal pressure drives growth of the cavities. Because of the occurrence of grain-boundary diffusion, the cavities located at the grain-boundary facets develop faster then cavities inside a grain. Also dislocation creep can contribute to the growth of the cavities. The grain boundary cavitation proceeds until the cavities coalesce to form a microcrack, and linking up of the microcracks leads to intergranular macroscopic failure.

Important earlier investigations of HA focussed on the evolution of one single cavity. Cylindrical or spherical unit cells containing one central cavity were investigated using analytical relations for the diffusive cavity growth, in some cases also accounting for creep deformations. In the analyses of Shih and Johnson [3] and Parthasarathy [4], only the internal pressure was taken into account. Later, Shewmon [5] included applied stress (perpendicular to the grain-boundary facet) in the model, which tends to accelerate cavity growth but, in this analysis, it was assumed that the cavity grows solely by grain-boundary diffusion. Building on earlier work [6,7], Van der Giessen et al. [8] presented a (partially) new cavity growth relation where diffusion and creep are coupled. The relation has been verified with extensive detailed numerical cell model analyses for all possible stress states which may be encountered under HA circumstances. In this way, the combined effect of the internal pressure and the remote applied stresses on cavity growth is incorporated. The relation has been applied in [2] to predict HA failure in 2.25Cr–1Mo steels.

* Corresponding author.

PII S0921-5093(96)10465-2

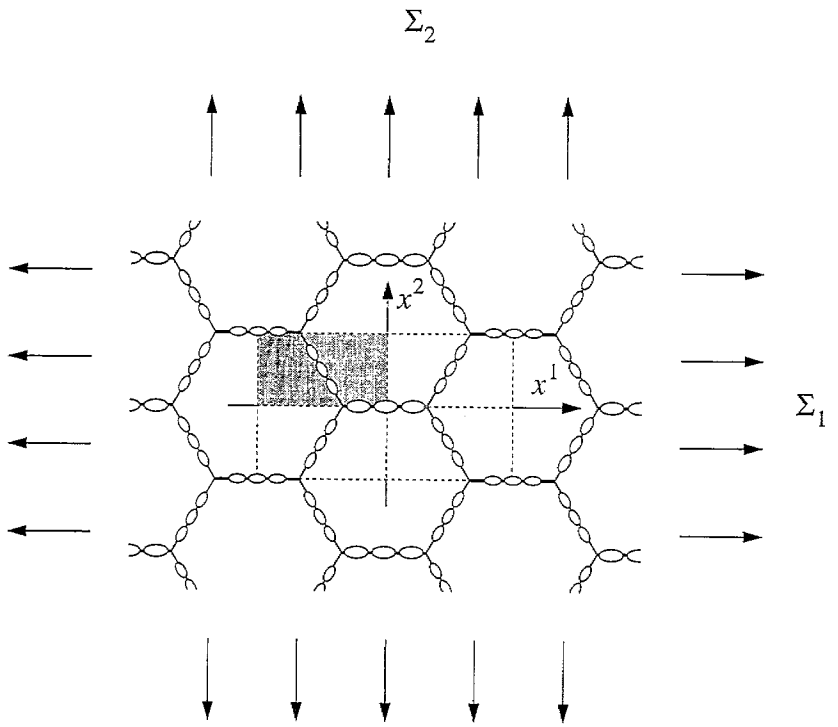

Fig. 1. Global coordinate system of the unit cell. Due to symmetries, only a quarter of the unit cell will be analyzed.

These single-cavity studies have given first indications on how HA develops in time. However, they imply that the cavities are distributed uniformly along the grain-boundary facets. In reality, carbides are not uniformly distributed over a grain facet and, more importantly, the carbides can have different compositions, leading to vast differences in the methane pressure of the gas that they may form ([2,5]). It is as yet not well understood what the influence is on HA of non-uniform distributions of microstructural properties, such as differences in reactivity of the carbide along a facet. In view of the possible variations in methane pressure distribution along a grain facet, compatibility of deformations is likely to lead to stress redistributions, similar to those associated with Dyson's [9] creep-constrained cavitation in creep rupture situations. As demonstrated in [9] and later confirmed in many other studies ([10,11]), grain-boundary cavitation in such cases is slowed down by the surrounding grains, which creep deform very slowly. Thus, the results of full field simulations of cavitation in a polycrystalline aggregate [10,11] were found to differ dramatically from the results obtained from a single-cavity model under the applied state of stress.

In order to investigate the effect on HA of microstructural variations as mentioned above, we make the scale transition from the level of individual cavities to the polycrystal level. For that purpose, the two-dimensional polycrystal model of Van der Giessen and Tvergaard [11] is extended for HA. Some preliminary

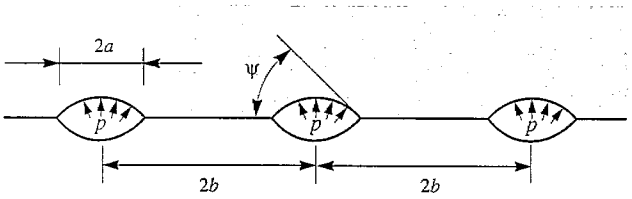

Fig. 2. Grain-boundary cavities having a diameter of $2a$ and which are spaced with a distance of $2b$. The growth of the cavities is driven by an internal pressure of p_m; it can however be accelerated or constrained by stresses remote from the cavity.

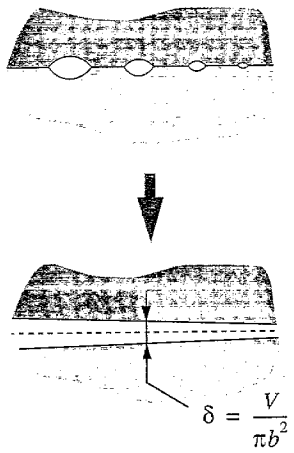

Fig. 3. Due to cavity growth the adjacent grains separate. This separation of grains δ can be quantified by 'smearing-out' of the cavity volume over its facet area.

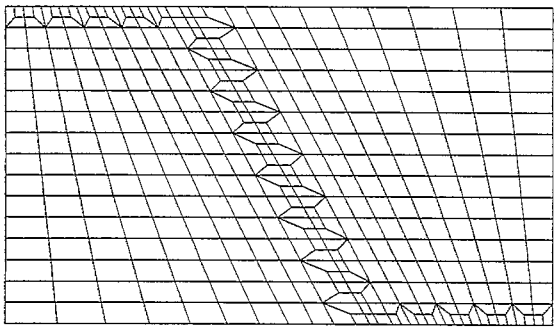

Fig. 4. Finite element mesh used for the numerical simulations of the quarter unit cell. Each quadrilateral consists of four triangular subelements. Grain-boundary elements are not shown.

explorations with this HA polycrystal model have been reported briefly in [12] and [13]. The objective of the paper is to draw up a complete picture of HA on the polycrystal scale and to provide an understanding of the influence of carbide variations under different relevant conditions.

The polycrystal model itself and the route to the numerical solutions are described in Sections 2 and 3. The model is then used to study non-uniform HA cavitation on two different size scales. First, in Section 4, internal cavity pressure variations are considered along grain-boundary facets, and next, in Section 5, internal cavity pressure variations over the polycrystal aggregate are studied. Two highly simplifying descriptions are discussed subsequently in Section 6 to try to better understand the results of the numerical simulations. These will be shown to capture some key aspects of the interactions that take place in the process of cavitation.

2. Polycrystal model for HA

At elevated temperatures in a hydrogen-rich environment, the hydrogen molecules dissociate into hydrogen atoms which diffuse into the material. While diffusing through the material, some hydrogen atoms will react with carbides present in the steel. During this reaction, methane molecules are formed which, contrary to the hydrogen atoms, cannot diffuse away through the metal. The (equilibrium) methane gas pressure in this reaction varies substantially with the stability of the carbide, and typically a material contains stable as well as unstable carbides. The equilibrium pressure for stable carbides is of the order of the applied stresses, whereas it can attain values that are orders of magnitudes larger than the applied stress for unstable carbides [2,14,15]. The ultimate internal pressure of the methane–hydrogen gas mixture, p_m, acting on the cavity surface consists of the partial methane pressure and the partial hydrogen pressure [2]:

$$p_m = p_{CH_4} + p_{H_2}. \quad (1)$$

Due to this internal pressure, a cavity can develop. The most important cavities are located on the grain-boundary facets, where they can develop rapidly by grain-boundary diffusion, assisted by dislocation creep. Since these grain boundary carbides cause the final intergranular failure, these are the only carbides taken into consideration. The grain boundary cavities grow until they coalesce and form a microcrack, and linking up of the microcracks leads to the macroscopic intergranular crack.

In this paper, it is assumed that hydrogen only reacts with the grain-boundary carbides that are present from the beginning. An implication of this assumption is that in our model no new cavities nucleate during HA. This appears to apply well for 2.25Cr–1Mo steels [16]. Another assumption made here is that the methane pressure is constant in time. However, Shih and Johnson [3] have reported that the equilibrium methane pressure will not always be reached in some cases at all moments. Hence, our considerations are expected to overestimate the actual cavity pressure and, hence, the cavity growth rate.

The polycrystal model of Van der Giessen and Tvergaard [11] is used here to simulate the HA process on grain-size scale. This model was initially developed to investigate creep rupture by grain-boundary cavitation, but since that process is closely related to HA the model can be easily adapted to study HA evolution. In the sequel, we shall only briefly describe the model, with an emphasis on those aspects that are new for the HA application; for details, we refer to [11].

The polycrystal model is based on a two-dimensional polycrystalline aggregate comprising hexagonal grains, as shown in Fig. 1. All grains are assumed here to have the regular hexagonal shape in the undeformed state with facet length $2R_I$. Periodicity in the microstructure of the polycrystal is exploited by constructing the aggregate on the basis of a unit cell. Assuming also a double microstructural symmetry inside the unit cell (see Fig. 1), only a quarter of the cell has to be

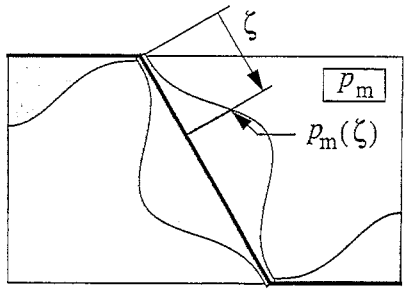

Fig. 5. The assumed internal cavity pressure p_m distribution along the grain-boundary facets for the results shown in Figs. 6–11 (p_m is plotted perpendicular to the facets), with a maximum value $p_m^{max} = 2.2\bar{p}_m$.

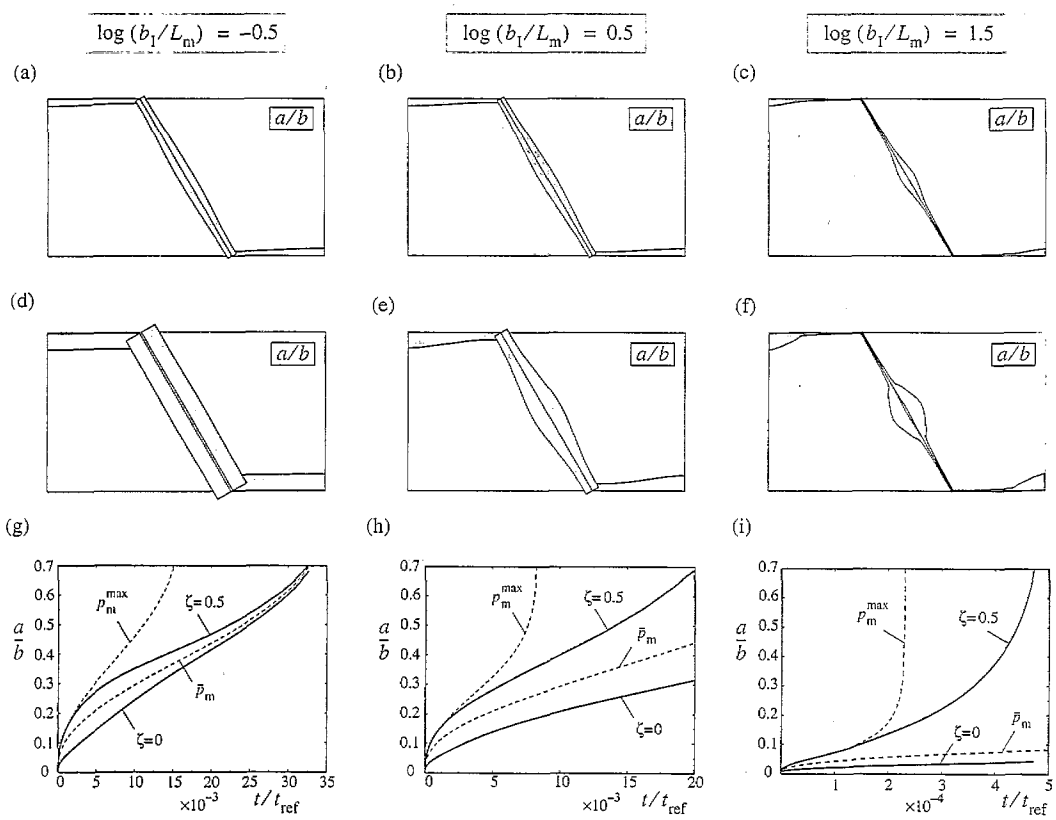

Fig. 6. Damage evolution for the cavity pressure distribution according to Fig. 5 for three values of b_I/L_m: (a)–(c) the damage state in terms of a/b (plotted normal to, and on either side of, the grain boundaries) for the three values of b_I/L_m when $(a/b)_{max} = 0.3$; (d)–(f) the damage state just prior to first cavity coalescence; (g)–(i) the damage evolution in time for two points along the grain facet (——). The single-cavity model results are shown by (– – –).

analyzed. In the x^1- and the x^2-direction of the global coordinate system, the polycrystal aggregate is subjected in general to macroscopic applied stresses Σ_1 and Σ_2, as shown in Fig. 1, under plane strain conditions.

The grains deform elastically as well as by Norton power-law creep in an isotropic manner. The constitutive equations are formulated in a finite strain formulation, using convected coordinates with metric coefficients g_{ij} and G_{ij} in the undeformed and deformed configurations, respectively. The covariant components of the Lagrangian strain tensor are denoted by η_{ij}, and the conjugate stresses are the contravariant components τ^{ij} of the Kirchhoff stress tensor on the current base vectors. The total strain rate $\dot{\eta}_{ij}$ is taken to be the sum of the elastic part $\dot{\eta}^e_{ij}$ and the creep part $\dot{\eta}^c_{ij}$. Thus, with the elastic stress–strain relationship $\overset{\nabla}{\tau}{}^{ij} = R^{ijkl}\dot{\eta}^e_{ij}$, in terms of the Jaumann stress-rate $\overset{\nabla}{\tau}{}^{ij} = \dot{\tau}^{ij} + (G^{ik}\tau^{jl} + G^{jk}\tau^{il})\dot{\eta}_{kl}$, the constitutive relations for the grain material can be written as

$$\overset{\nabla}{\tau}{}^{ij} = R^{ijkl}(\dot{\eta}_{kl} - \dot{\eta}^c_{kl}) \tag{2}$$

with

$$\dot{\eta}^c_{ij} = \dot{\varepsilon}^c_e \frac{3}{2}\frac{s_{ij}}{\sigma_e}, \tag{3}$$

where σ_e is the effective Mises stress, $\sigma_e = \sqrt{3s_{ij}s^{ij}/2}$, and the stress deviator components are defined by $s^{ij} = \tau^{ij} - G^{ij}\sigma_m$ with the mean stress defined by $\sigma_m = \tau^k_k/3$. The effective creep strain rate $\dot{\varepsilon}^c_e$, according to the Norton power law, is given by

$$\dot{\varepsilon}^c_e = \dot{\varepsilon}_0\left(\frac{\sigma_e}{\sigma_0}\right)^n. \tag{4}$$

Here, σ_0 is a reference stress parameter, $\dot{\varepsilon}_0$ is a reference strain-rate parameter and n is the creep exponent.

A spherical-caps-shaped cavity along a facet can be characterized by its radius a and its equilibrium tip angle ψ (see Fig. 2). The separation between two neighbouring cavities is $2b$. The volume of a cavity is $V = \frac{4}{3}\pi a^3 h(\psi)$, where the function $h(\psi)$ is the geometrical cavity shape parameter defined as $h(\psi) = ((1+\cos\psi)^{-1} - \frac{1}{2}\cos\psi)/\sin\psi$.

At temperatures typical for HA, cavities grow by grain-boundary diffusion and by creep of the adjacent grain material. Thus, the volumetric cavity growth rate $\dot{V}$ consists of a part due to grain-boundary diffusion, $\dot{V}_{diff}$, and a part due to creep, $\dot{V}_{cr}$, i.e., $\dot{V} = \dot{V}_{cr} + \dot{V}_{diff}$. Growth is driven by the gas pressure p_m inside the cavity, but can be accelerated or slowed down by stresses remote from the cavity, as characterized by σ^{rc}_n,

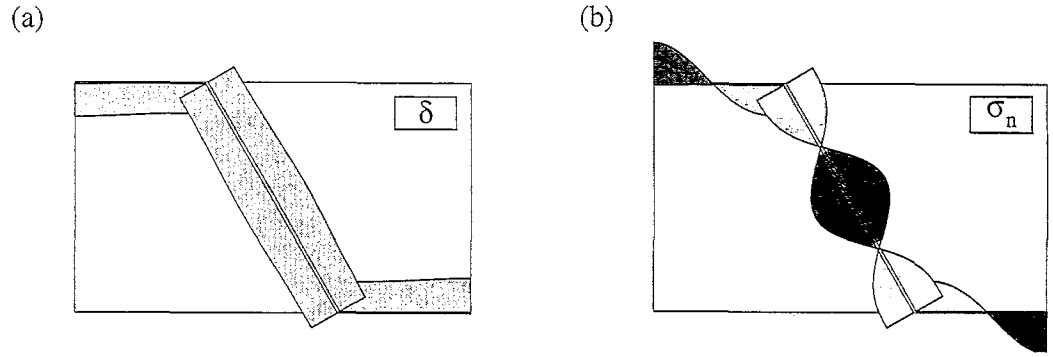

Fig. 7. Distributions of (a) the grain separation δ, normalized by the current maximum value $\delta_{max} = 3.0 \times 10^{-2} R_I$, and (b) the normal stress $\sigma_n/\bar{p}_m$ just prior to first cavity coalescence for $\log(b_I/L_m) = -0.5$. The darker areas in (b) indicate that the normal stress is compressive.

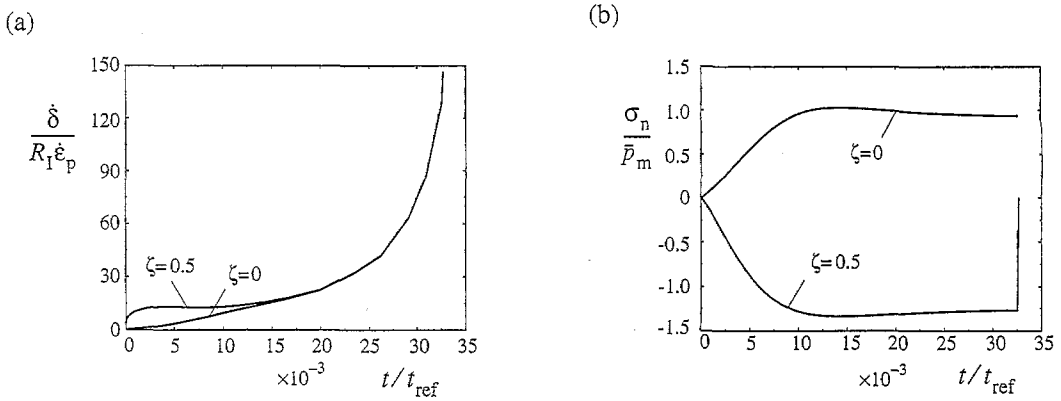

Fig. 8. Evolution of (a) the separation rate, normalized with the initial facet half-width R_I and the creep rate parameter $\dot{\varepsilon}_p$ (see Eq. (13)), and (b) the normal stress $\sigma_n/\bar{p}_m$ at the triple point $\zeta = 0$ and the center fo the facet $\zeta = 0.5$, for the case where $\log(b_I/L_m) = -0.5$ (see Fig. 7).

σ_e^{rc} and σ_m^{rc}, being the average stress normal to the grain boundary facet, the average Mises effective stress and the average mean stress remote from the cavity, respectively. To determine the volumetric growth rate, a single cavity has been analyzed numerically, first by Needleman and Rice [6] for remote uniaxial stress states, and by Sham and Needleman [7] for stress triaxialities witnessed at macroscopic cracks or notches. These analyses have been extended by van der Giessen et al. [8] to cover all possible axisymmetric stress states. This elaboration was necessary because in the case of HA, the cavity may grow solely due to the internal cavity pressure, which can be classified as cavity growth under a purely hydrostatic stress state. The numerical results could be captured fairly well by approximate analytical relations which have been presented in their most complete form in [2]. Only a summary of the relations will be given; more details can be found in the above references.

When the cavity grows by creep, two different creep growth modes can be distinguished [8]: a mode which can be associated with low stress triaxialities and/or low porosities (i.e., small values of a/b) and a second mode which can be associated with high stress triaxialities and/or high porosities. The volumetric growth rate by creep for the first mode, according to [2] and [8] is given by

$$\dot{V}_{cr}^{L} = 2\pi\dot{\varepsilon}_m a^3 h(\psi)\,\mathrm{sign}(\sigma_m)\left[\alpha_n + \beta_n\left|\frac{\sigma_e}{\sigma_m}\right|\right]^n \quad \text{if } |\sigma_m/\sigma_e| \geq 1; \tag{5}$$

$$\dot{V}_{cr}^{L} = 2\pi\dot{\varepsilon}_m a^3 h(\psi)\,\mathrm{sign}(\sigma_m)[\alpha_n + \beta_n]^n\left|\frac{\sigma_e}{\sigma_m}\right|^{n-1} \quad \text{if } |\sigma_m/\sigma_e| < 1, \tag{6}$$

where the shorthand notation $\dot{\varepsilon}_m = \dot{\varepsilon}_0|\sigma_m/\sigma_0|^n$ is introduced, and where $\sigma_m = \sigma_m^{rc} + p_m - 2T_s(\sin\psi)/a$. Here, T_s is the surface tension and σ_e is equal to the remote effective stress σ_e^{rc}. The constants α_n and β_n are defined by $\alpha_n = 3/(2n)$ and $\beta_n = (n-1)(n+0.4319)/n^2$. Finally, $\mathrm{sign}(\sigma_m)$ denotes the sign of σ_m. In case of the second creep growth mode, for high porosities or stress triaxialities σ_m/σ_e, the volumetric growth rate is given by

$$\dot{V}_{cr}^{H} = 2\pi\dot{\varepsilon}_m a^3 h(\psi)\,\mathrm{sign}(\sigma_m) \times \left[\frac{1}{1-(0.87a/b)^{3n}}\left(\alpha_n + \frac{1}{n}\frac{\mathrm{sign}(\sigma_n^{rc} - \sigma_m^{rc})}{\mathrm{sign}(\sigma_m)}\left|\frac{\sigma_e}{\sigma_m}\right|\right)\right]^n \quad \text{if } |\sigma_m/\sigma_e| \geq 1; \tag{7}$$

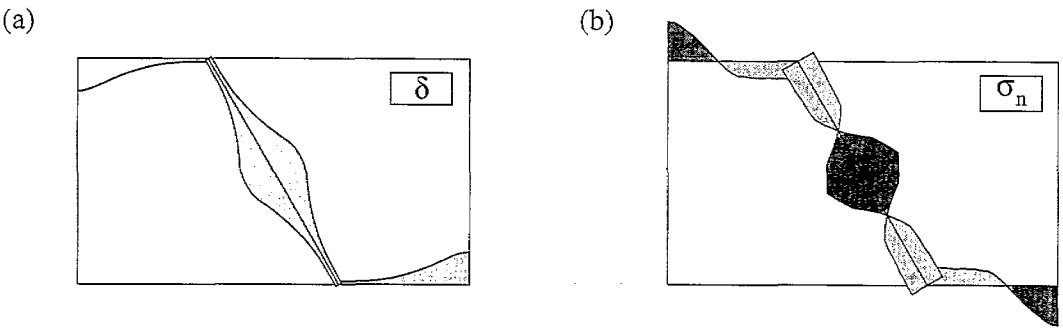

Fig. 9. Distribution of (a) the separation δ/δ_{max}, where $\delta_{max} = 2.7 \times 10^{-2} R_I$, and (b) the normal stress $\sigma_n/\bar{p}_m$ just prior to first cavity coalescence for $\log(b_I/L_m) = 0.5$. The darker areas in (b) indicate that the normal stress is compressive.

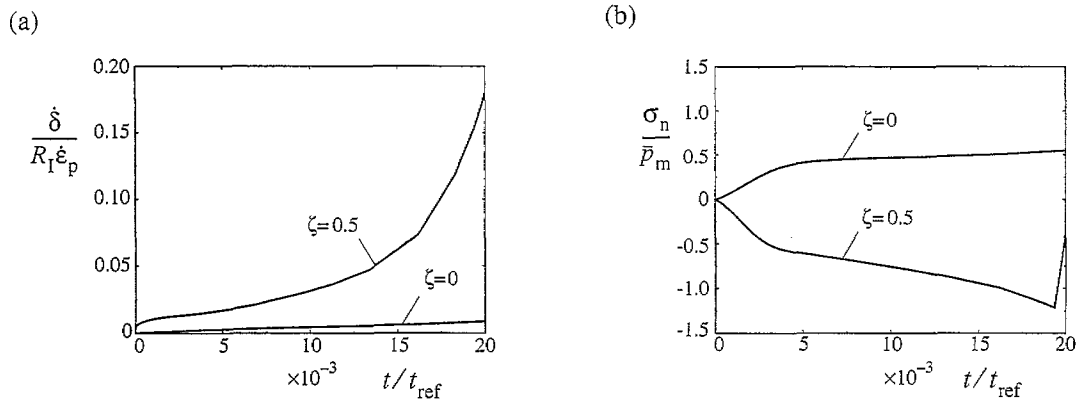

Fig. 10. Evolution of (a) the separation rate and (b) the normal stress at the triple point $\zeta = 0$ and the center of the facet $\zeta = 0.5$ for the case where $\log(b_I/L_m) = 0.5$ (see Fig. 9).

$$\dot{V}_{cr}^{H} = 2\pi\dot{\varepsilon}_m a^3 h(\psi)\,\mathrm{sign}(\sigma_m) \times \left[\frac{1}{1-(0.87a/b)^{3/n}}\left(\alpha_n + \frac{1}{n}\frac{\mathrm{sign}(\sigma_n^{rc}-\sigma_m^{rc})}{\mathrm{sign}(\sigma_m)}\right)\right]^n \times \left|\frac{\sigma_e}{\sigma_m}\right|^{n-1} \quad \text{if } |\sigma_m/\sigma_e| < 1. \tag{8}$$

The expression for the volumetric growth rate $\dot{V}_{diff}$ for growth by grain-boundary diffusion is a modification of the Hull and Rimmer [17] result for rigid grains, improved for the coupling with creep in the grains [6,7]. With the extension for the internal cavity pressure p_m given in [8], the diffusive growth rate is given by

$$\dot{V}_{diff} = 4\pi\mathscr{D}\frac{\sigma_n^{rc} + p_m - (1-f)2\gamma_s \sin\psi/a - f2T_s \sin\psi/a}{\ln(1/f) - \frac{1}{2}(3-f)(1-f)}, \tag{9}$$

where the grain boundary diffusion parameter $\mathscr{D} = D_B\delta_B\Omega/k\Theta$ depends on the boundary diffusivity $D_B\delta_B$, on the atomic volume Ω and the energy per atom measure $k\Theta$. The diffusive growth is driven by the average stress normal to the grain-boundary facet σ_n^{rc} in addition to the internal cavity pressure p_m. The free surface energy γ_s and the surface tension T_s commonly result in a sintering effect, expressed through a sintering stress $\sigma_s = (1-f)2\gamma_s \sin\psi/a + f2T_s \sin\psi/a$. However, as soon as the cavity can open and develop, the sintering stress σ_s has hardly any effect on the further evolution [2]. Therefore, both the free surface energy γ_s and the surface tension T_s are neglected in the analysis by putting $\sigma_s = 0$. The parameter f in Eq. (9) is determined by the diffusive path length L_{diff} and the cavity radius a by

$$f = \left(\frac{a}{L_{diff}}\right)^2.$$

When creep in the grains is negligible, the diffusive path length L_{diff} is equal to the cavity half-spacing b. However, when the creep deformations in the vicinity of the cavity become of the same order of magnitude as the diffusional deformations along the facet [6], then the diffusive path length shortens, so that the volumetric growth rate $\dot{V}_{diff}$ increases. The type of interaction between creep deformations and the diffusional process depends on the creep modes (indicated with superscript H and L); Van der Giessen et al. [8] have shown that

$$\dot{V}_{diff}^{L} = \dot{V}_{diff}(f), \quad f = \max\left[\left(\frac{a}{b}\right)^2, \left(\frac{a}{a+1.5L}\right)^2\right];$$

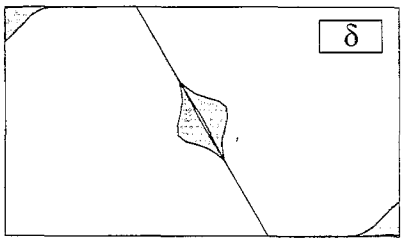

Fig. 11. Distribution of the grain separation δ, normalized by the current maximum value $\delta_{max} = 3.1 \times 10^{-2} R_I$, just prior to first cavity coalescence for $\log(b_I/L_m) = 1.5$.

$$\dot{V}^{H}_{diff} = \dot{V}_{diff}(f), \quad f = \left(\frac{a}{b}\right)^2$$

is a fair approximation. Here, $L = (\mathscr{D}\sigma_e/\dot{\varepsilon}^c_e)^{1/3}$ $(\sigma_e \neq 0)$ is a stress- and temperature-dependent length parameter, first introduced by Needleman and Rice [6]. The ultimate volumetric growth rate $\dot{V}$ is obtained from Eqs. (5)–(9) as

$$|\dot{V}| = \max[|\dot{V}^{L}_{cr} + \dot{V}^{L}_{diff}|, |\dot{V}^{H}_{cr} + \dot{V}^{H}_{diff}|]. \tag{10}$$

The surface diffusion is assumed to be rapid enough to maintain the spherical-caps shape of the cavity. This shape assumption seems to be consistent with the observations for 2.25Cr–1Mo steel by Shewmon [16]. Then the growth rate of the cavity radius a is given by

$$\dot{a} = \frac{\dot{V}}{4\pi a^2 h(\psi)}$$

with $\dot{V}$ according to Eqs. (5)–(10).

Due to the growth of the cavities, the adjacent grains separate. If all cavities have the same size and the same spacing, this average separation δ is determined by

$$\delta = \frac{V}{\pi b^2}$$

In a schematic way, Fig. 3 depicts a variation in the separation δ along the grain-boundary facet as a result of differences in, e.g., cavity volume. Differentiating with respect to time gives the average separation rate $\dot{\delta}$

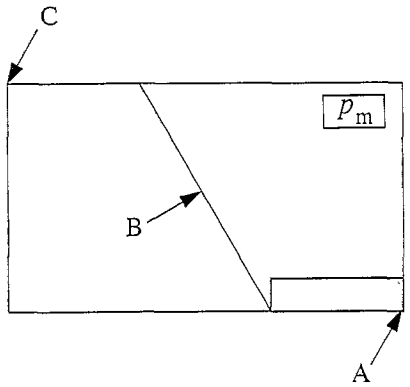

Fig. 13. Internal cavity pressure distribution over the quarter unit cell. Only the cavities along the central facet are pressurized. On the other facets the internal cavity pressures are assumed to be zero.

$$\dot{\delta} = \frac{\dot{V}}{\pi b^2} - \frac{V}{\pi b^2} 2\frac{\dot{b}}{b} = \frac{\dot{V}}{\pi b^2} - \delta \dot{\varepsilon}_n. \tag{11}$$

Thus, the separation rate is a function of the cavity growth rate $\dot{V}$ and of creep deformations in the plane of the facet, expressed in the second term in the right-hand side. The average separation rate $\dot{\delta}$ will vary along the facet as a consequence of variations caused by variations of cavity distributions and by variations in the volumetric growth rate. The latter are due mainly to variations of the internal driving pressure p_m due to different carbide compositions [2], to variations in cavity size, and to a non-uniform remote stress distribution along the facet.

Creep in polycrystalline metals may be accompanied by grain-boundary sliding [18]. However, in materials that have failed by HA, grain-boundary sliding has not been observed. This may be due to the temperature levels at which HA-susceptible materials are applied and also to the presence of a high density of carbides on the grain boundaries which tend to act as obstacles for sliding. Therefore, grain-boundary sliding is not incorporated into the model.

In the model, a microcrack will form when cavities coalesce at $a/b = 1$. However in reality, grain-boundary

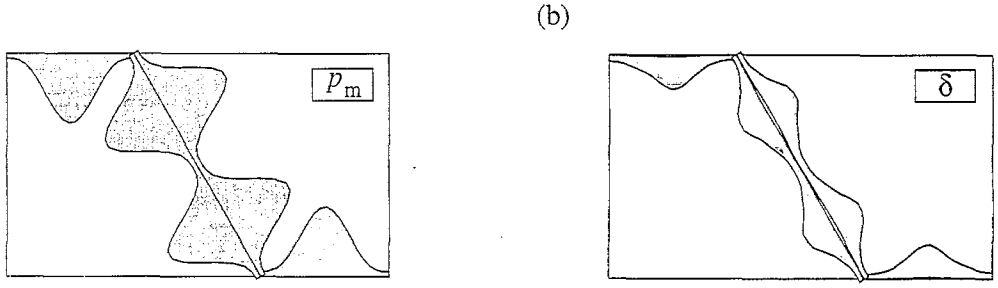

Fig. 12. (a) The assumed short wavelength, internal cavity pressure distribution over the polycrystal; (b) the separation distribution δ/δ_{max}, where $\delta_{max}/R_I = 3.1 \times 10^{-2}$, for $\log(b_I/L_m) = 0.5$ just prior to first cavity coalescence.

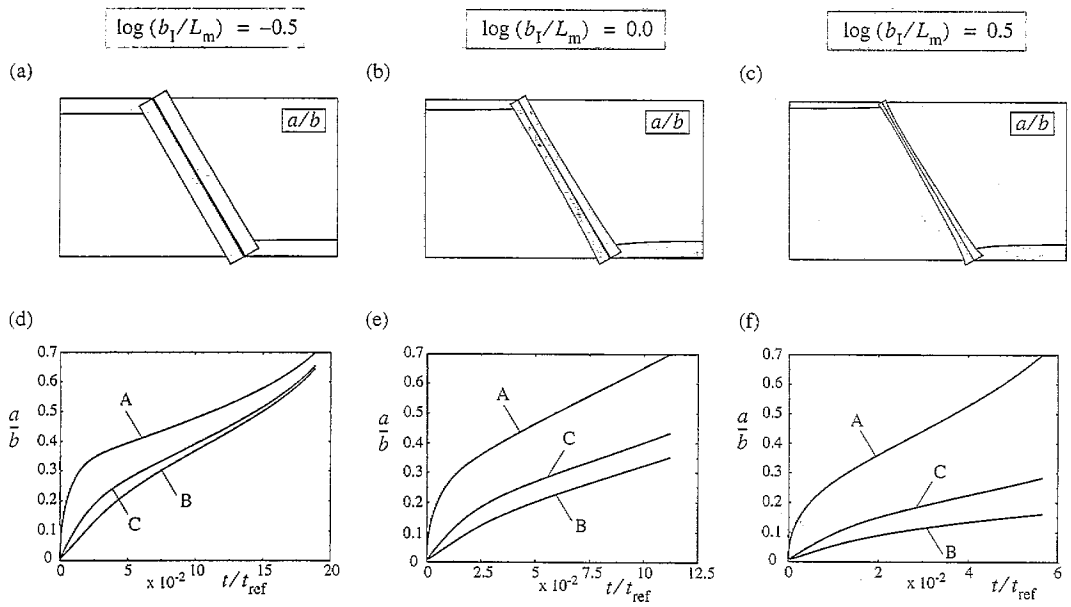

Fig. 14. (a)–(c) The damage state in terms of a/b for three different values of b_1/L_m just before first cavity coalescence. The evolution of the damage at the facet midpoints A, B and C (see Fig. 13) are shown in (d)–(f).

failure by cleavage of the ligament is expected to occur earlier, this in analogy with creep ruptures by cavitation [18]. It is assumed here that failure takes place at $a/b = 0.7$. However the precise value of a/b is not very important for the ultimate time to failure, as cavity growth accelerates strongly at such large values of a/b.

The results obtained with the polycrystal model will be compared with a single cavity model as discussed in detail in [2]. This model boils down to directly subjecting the representative cavity to the macroscopic stresses Σ_1 and Σ_2. The cavity growth relations in the single-cavity model are the same as presented above, but with σ_n^{rc}, σ_e^{rc} and σ_m^{rc} being replaced by Σ_2, $\frac{1}{2}\sqrt{3}|\Sigma_2 - \Sigma_1|$ and $\frac{1}{2}(\Sigma_2 + \Sigma_1)$, respectively. The difference between cavitation in the single-cavity model and in the polycrystal model is that, in the latter, the increase in cavity volume has to be accommodated by deformations of the surrounding grains. The creep resistance of the grains may constrain the volume cavity growth rate and, therefore, the cavitation evolution. This concept of creep-constrained cavity growth was pointed out by Dyson [9] for cavitation under circumstances leading to intergranular creep rupture, but is expected to apply equally well here. In the single-cavity model, these kinds of interactions with adjacent grains are not present and, therefore, in the single-cavity model, cavity growth is unconstrained.

3. Method of analysis

The numerical method used to solve the problem discussed above is largely similar to that in [11] and [19]. In this section, we therefore only give a brief summary and refer to [19] for more details.

The grains themselves are discretized by quadrilateral finite elements, each one of which consists of four triangular constant strain elements in a 'crossed triangle' configuration. The finite element grid used is depicted in Fig. 4. The HA and resulting grain-boundary cavitation process is incorporated through grain-boundary elements. In this case, the only deformation mode for these interface-type elements is the grain separation δ. Consistent with the finite element representation inside the grains, the grain-boundary elements use linear interpolations for δ and for the other grain boundary characteristics, such as cavity size a and spacing b. For computational convenience, a layer of linear elastic springs is added to the grain-boundary elements with a normal stiffness k_n, so that the local normal stress σ_n at the grain boundary is determined through

$$\dot{\sigma}_n = k_n(\dot{\delta}_{gb} - \dot{\delta}). \tag{12}$$

Here, δ_{gb} is the actual separation and δ is the separation due to cavitation, as being governed by the evolution Eq. (11). A large value of the stiffness k_n ensures that the deviation $\delta_{gb} - \delta$ remains small; here, we have used $k_n = 10E/R$, where E is the Young's modulus.

The governing equations for the grains as well as for the grain boundaries are solved in a linear incremental manner. The remote normal stress σ_n^{rc} to be used in the cavity growth Eqs. (5)–(9) is taken from the grain boundary stress, i.e., $\sigma_n^{rc} = \sigma_n$. The remote effective and

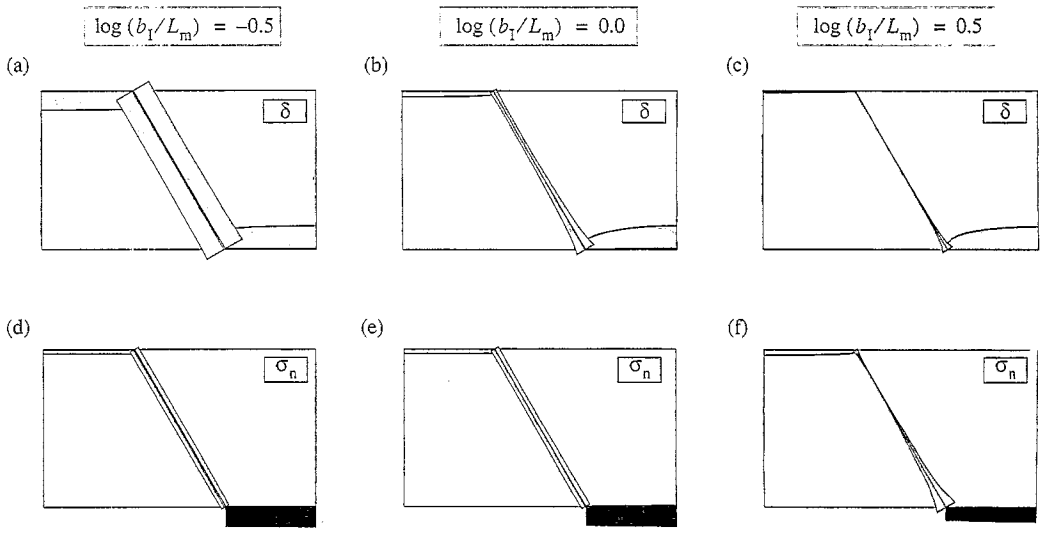

Fig. 15. Distribution of (a)–(c) the separation δ/δ_{max} and (d)–(f) the normal stress $\sigma_n/\bar{p}_m$ over the polycrystal for different b_I/L_m (see Fig. 14). The maximum separations δ_{max} are (a) and (b) $3.1 \times 10^{-2} R_I$, and (c) $2.9 \times 10^{-2} R_I$. At the darker areas in (d)–(f), the normal stress is compressive.

mean stress, σ_e^{rc} and σ_m^{rc}, are evaluated as averages from the corresponding stresses in the grain elements adjacent to the grain boundary. To increase the numerical stability of the procedure, a forward gradient approach is used to integrate the constitutive relations, Eqs. (2) and (12). Finite strains are accounted for in the analyses, but in the present applications the strains remain below a few percent.

The symmetries imposed on the quarter cell imply that the (quarter) cell boundaries remain straight throughout the process, and shear stress free. Therefore, uniform displacement rates are prescribed in the x^1 and x^2 directions so that the average true stresses Σ_1 and Σ_2, respectively, retain specified constant values in time.

4. Variations along grain boundaries

In this section, the influence of non-uniformities in internal cavity pressure on the scale of grain boundaries will be investigated. All grain-boundary facets in the polycrystal have the same uniform carbide distribution, but the reactivity of the carbides and therefore their resulting internal cavity pressure p_m are taken to vary along the facet. The uniform cavity distribution along a facet is characterized by the initial cavity spacing relative to the facet length as $(b/R)_I = 0.1$. The initial cavity size is taken to be $(a/b)_I = 0.01$. In all cases, the Poisson ratio $\nu = 0.33$, the cavity tip angle $\psi = 75°$, and the creep exponent $n = 5$. To describe the variation of the internal cavity pressure over the facet, a local coordinate ζ is introduced along the grain boundary, ranging between 0 and 1. The first internal cavity pressure distribution we are considering is characterized by $p_m(\zeta)/\bar{p}_m = 2.0 \sin^3(\pi\zeta) + 0.16$ with $\bar{p}_m/E = 1.0 \times 10^{-3}$, and is shown graphically in Fig. 5. It is assumed that there are no macroscopic stresses, $\Sigma_1 = \Sigma_2 = 0$, so that HA is solely driven by the internal cavity pressure. Note that because of symmetry, cavitation damage will develop equally on each grain-boundary facet.

The various parameters for creep and diffusion are expressed through the dimensionless group b_I/L_m, where L_m is defined by

$$L_m = \left[\frac{\mathscr{D}\bar{p}_m}{\dot{\varepsilon}_p}\right]^{1/3} \quad \text{where } \dot{\varepsilon}_p = \dot{\varepsilon}_0 \left(\frac{\bar{p}_m}{\sigma_0}\right)^n. \tag{13}$$

In practice [2], the value of this parameter can range from $\log(b_I/L_m) = -2$, where cavitation is completely dominated by diffusion, up to around $\log(b_I/L_m) = 2$, where the creep contribution to cavity growth is most important. Within this range, three parameter values are taken: (i) $\log(b_I/L_m) = -0.5$, where cavity growth is diffusion dominated; (ii) $\log(b_I/L_m) = 0.5$, where diffusive cavity growth is expected to interact with creep, and finally (iii) $\log(b_I/L_m) = 1.5$, where cavitation is creep dominated. To follow the cavity evolution in time, a reference time scale is introduced by $t_{ref} = b_I^3/(\mathscr{D}\bar{p}_m)$, which is based on the diffusive cavity growth process.

An obvious important parameter to look at is grain-boundary damage in terms of a/b. For the three cases, the damage evolution is shown in Fig. 6. In Fig. 6(a)–(c) the a/b distribution is depicted when a/b reaches the value of 0.3 at the center of the facets (i.e., at about half the ultimate damage). It can be seen that the damage distribution tends to become more non-uni-

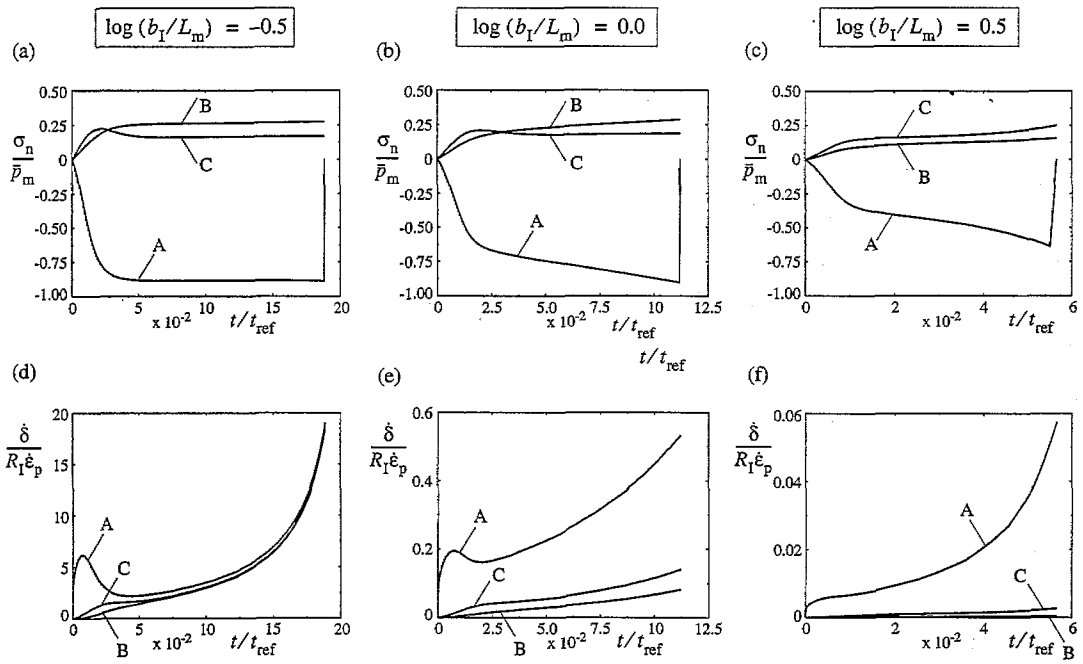

Fig. 16. Evolution of the separation rates and the normal stress at A, b and C (see Fig. 13) for the different cases shown in Figs. 14 and 15.

form for higher b_I/L_m, i.e., when the creep rate (relative to the diffusional rate) increases. In Fig. 6(d)–(f), the damage distribution is depicted when first coalescence of cavities occurred ($a/b = 0.7$) and it is seen that the three distributions differ significantly. In Fig. 6(d), the cavity-size distribution is virtually uniform, whereas this uniformity has faded in Fig. 6(e), and is strongly non-uniform in Fig. 6(f). To compare these polycrystal results with the single-cavity model predictions, the damage evolution in the middle and at the triple point of a facet are plotted in Fig. 6(g)–(i). The single-cavity model prediction is shown for an internal cavity pressure of $p_m = 2.2\bar{p}_m$ (which corresponds with the maximum internal cavity pressure along a facet), as well as for an internal pressure which corresponds to the average internal pressure $\bar{p}_m$. Notice that the differences in damage evolution under these different internal cavity pressures increase strongly with increasing relative importance of the creep growth rate. In all three cases, unconstrained growth of the single cavity under the peak cavity pressure is faster than growth at the facet center in the polycrystal, even in Fig. 6(i), where the creep rate inside the grains is relatively large. The single-cavity model results, when the cavity is subjected to the average internal pressure, are always in between the polycrystal results at facet center and triple point.

In order to further elucidate the origin of the phenomena observed above, it seems appropriate to also investigate the grain separation $\delta(\zeta)$ or the separation rate $\dot{\delta}(\zeta)$ along the facet. The reason is that it is the difference in separation rate between a cavity and its neighbouring cavities that must be accommodated by deformations of the adjacent grains. When the resistance of the grains to such deformations is large, stress redistributions inside the grains will take place, leading to 'reactive' stresses acting on the grain-boundary facet, such that compatibility is assured. Even though the present setting for HA is somewhat different, this phenomenon of internal stress redistributions is similar to that underlying Dyson's [9] concept of creep constraints on creep rupture. Therefore, we also investigate the evolution of the facet normal stress distribution $\sigma_n(\zeta)$ over the facets.

For the first case where $\log(b_I/L_m = -0.5$, it can be seen in Fig. 7(a) that the average grain separation is nearly uniform at the moment of first coalescence. This indicates that all cavities have grown at nearly the same rate. This is possible only when the cavity growth rate due to the internal pressure is partially counteracted in some regions or accelerated by normal stresses in other regions, in such a way that the grain separation rate $\dot{\delta}(\zeta)$ becomes uniform along the facets. In the middle of the grain boundary, a compressive stress constrains the evolution, whereas close to triple points growth is accelerated by tensile normal stress, as can be seen in Fig. 7(b). In this case, where diffusion is much faster than creep, there is insufficient time for the grain to creep deform significantly to accommodate the non-uniform separation rates caused by the cavity pressure only. As a consequence, as shown in Fig. 8(a), the average

separation rates near the triple point and in the middle of the grain boundary are virtually identical, except for an initial transient. Fig. 8(b) shows the development in time of tensile stresses near the triple point and of the compressive stresses in the middle of the facet. After an elastic transient, the normal stresses stabilize in time, and the grains separate as virtually rigid bodies.

In the next case, for $\log(b_I/L_m) = 0.5$, the creep rate is increased relative to the diffusional rate. Note that the separation distribution δ in Fig. 9(a) is much more non-uniform than in the case for $\log(b_I/L_m) = -0.5$ in Fig. 7(a). Now, there has been sufficient time for the grains to deform by creep flow, thus accommodating the variations in separation rate. At the same time, the magnitude of the normal stresses is seen to be somewhat lower (see Fig. 9(b)). Comparing the separation rates throughout the process as shown in Fig. 10(a), with the previous results in Fig. 8(a), we see that the separation rates in the center and at the triple point of a facet now differ significantly. The evolution of the normal stresses shown in Fig. 10(b) indicate that stress redistributions take place throughout the process, but the stress levels remain below those in Fig. 8(b). The normal stress is still of importance in this case since cavity growth is still mainly diffusion controlled.

When $\log(b_I/L_m) = 1.5$, this is no longer the case. Diffusion is hardly of importance anymore and the process is fully creep dominated. This leads to relatively large creep deformations of the grains in the neighbourhood of the highest cavity pressure, as shown clearly in Fig. 11, demonstrating the strongly non-uniform separation distribution along the grain-boundary facet. In this creep-dominated case, facet normal stresses have lost their importance for cavity growth, but now the distributions of mean stress and effective stress near the grain boundary are of primary importance, as can be concluded from the growth relations, Eqs. (5)–(8). The magnitude of these stresses is much smaller than the stresses built up in the previous cases, but due to the highly non-linear creep relations, these small stresses still result in a significant effect on time to first coalescence compared with fully unconstrained growth, as we have seen in Fig. 6(i).

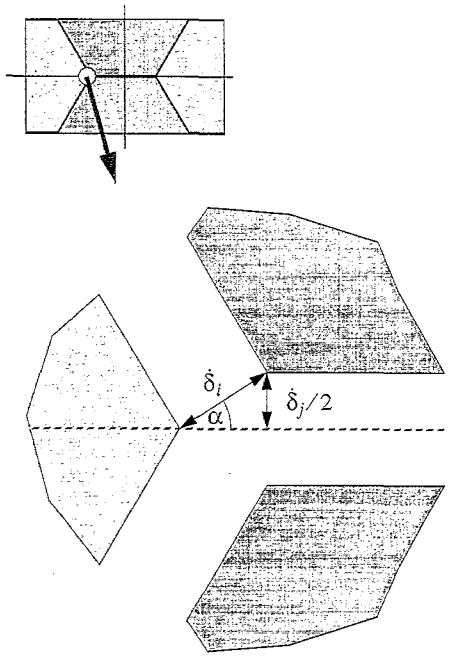

Fig. 17. Close-up of a triple point when the creep deformability of the grains is negligible: the separation rates $\dot{\delta}_i$ and $\dot{\delta}_j$ on adjacent facets are kinematically coupled.

The previous results have shown that, depending primarily on b_I/L_m, non-uniform cavity pressure distributions over grain facets can lead to substantial normal stresses over the grain facets, even though there is no externally applied stress. In these cases, the normal stress distribution has to be self-equilibrated, and leads to compressive stresses in the neighbourhood of high cavity pressures and tensile stresses elsewhere. This has been seen to lead to constrained growth of the cavities that have relatively high internal gas pressures, and accelerated growth of cavities under low internal pressure. Thus, facet regions of high gas pressure seem to 'interact' with regions of low pressure through continuous redistributions of normal stress over the facets. An apparent measure of this interaction is the maximum value of $|\sigma_n/\bar{p}_m|$ occurring anywhere along the facet: the larger this ratio, the higher the interaction and the stronger the tendency for uniform separation along the facet.

By changing the wavelength of the methane distribution, it is investigated if the magnitude of this interaction is dependent on the length scale of the pressure distribution. Fig. 12(a) depicts a distribution of the internal cavity pressure p_m with half the period of the variations, as given by $p_m(\zeta)/\bar{p}_m = 2.0|\sin^3(\pi 2\zeta)| + 0.16$. The previous calculations have been repeated for this distribution for the intermediate value $\log(b_I/L_m) = 0.5$. Comparing the separation at the time of first coalescence, shown in Fig. 12(b), with Fig. 9(a), it is observed that the shorter wavelength distribution leads to somewhat more uniform cavitation. This suggests that interaction increases with decreasing wavelength in the methane distribution.

The restriction of using grain-boundary elements in the polycrystal model is that only gradients in grain-boundary properties along a facet can be accounted for in the analyses. It is not possible to model a single aggressive carbide surrounded by relatively harmless carbides, which may happen in practice. However, especially for these cases, where the grain material creeps severely, one can rely on the single-cavity relation expressed in Eqs. (5) and (6). This is possible because

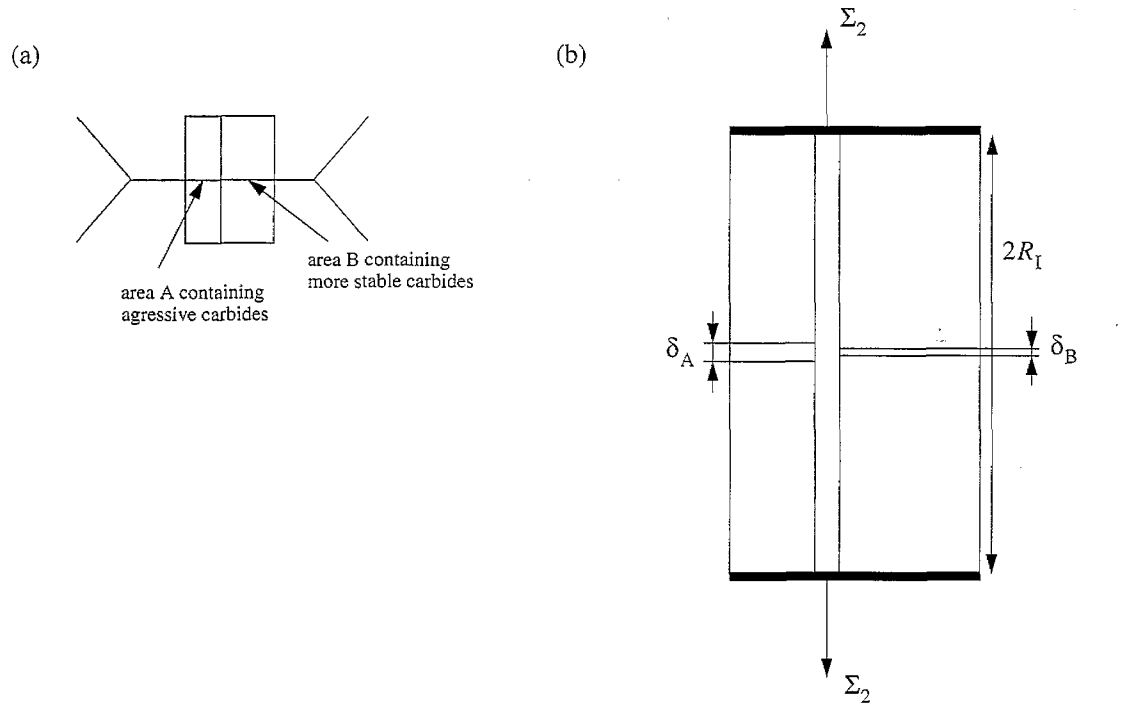

Fig. 18. (a) Schematic motivation for the two-bar model along a grain boundary facet. (b) The two-bar model: a parallel arrangement of two coupled bars with different cavitation properties.

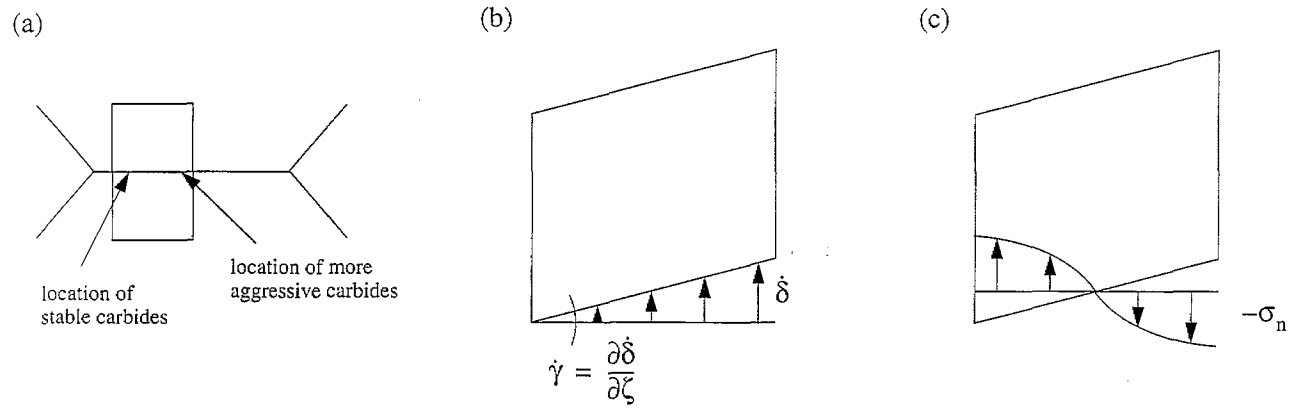

Fig. 19. (a) Variations in the internal cavity pressure along a grain-boundary facet due to differences in carbide reactivity, (b) leading to a non-uniform separation rate distribution with gradient $\dot{\gamma}$ to be accommodated by the adjacent grain material, and (c) the resulting reactive normal stresses on the grain boundary.

these relations govern the volumetric growth rate of a cavity in an infinite creeping medium. The cavity spacing b is irrelevant in those cases.

5. Variations over the polycrystalline aggregate

In this section, we consider non-uniformities in the internal cavity pressure distribution over the polycrystalline aggregate. In contrast with the previous section, the internal pressure is now constant along any facet, but can differ from facet to facet. Only a single representative microstructure is considered, shown in Fig. 13, as this highlights the issues involved. More complex microstructures have been considered in [12,13]. The central facet in the unit cell is taken to contain relatively aggressive carbides, characterized by $p_m/E = 1.0 \times 10^{-3}$, whereas on the other facets the carbides are assumed to be harmless; the carbide density and the initial cavity sizes are taken to be the same as on the central facet, but their internal pressure p_m is taken to be negligible, i.e., $p_m = 0$ for convenience. In this section, the parameter

b_I/L_m is taken to vary from $\log(b_I/L_m) = -0.5$ to $\log(b_I/L_m) = 0.5$. All other parameter values are kept the same as above, including the assumption that no macroscopic stresses are applied, $\Sigma_1 = \Sigma_2 = 0$.

In Fig. 14(a)–(c), the distribution of the damage parameter a/b over all facets is plotted just prior to first cavity coalescence. In Fig. 14(a), where $\log(b_I/L_m) = -0.5$, the a/b distribution has developed to become virtually uniform. In Fig. 14(b), where the creep rate is enhanced relative to the diffusional rate, $\log(b_I/L_m) = 0.0$, the a/b distribution has become slightly non-uniform, while in Fig. 14(c), where the creep rate is even faster, $\log(b_I/L_m) = 0.5$, the central facet is nearly completely cavitated, whereas on the inclined facet nearly no damage has developed. Note that the parallel top facet in the quarter unit cell, which is further away from the central cavitating facet than the inclined facet is, has cavitated more. Hence, the interaction (in the sense of the previous section) with the top facet has been stronger than with the adjacent inclined facet. In Fig. 14(d)–(f), the evolution of a/b at the midpoint of each facet is shown. These results seem to give additional evidence for the fact that the interaction with the neighbouring facets decreases with increasing value of b_I/L_m. Notice that in the case of vanishingly small interaction, cavitation on the facets with the non-aggressive carbides would not develop at all.

The interactions referred to here are again most clearly demonstrated by the distributions of the separation δ and of the facet normal stress σ_n. As shown in Fig. 15(a), the separation distribution for $\log(b_I/L_m) = -0.5$ is almost perfectly uniform, indicating rigid grain behaviour. With increasing b_I/L_m, Fig. 15(b)–(c), the δ distribution becomes more and more non-uniform over the unit cell by significant creep deformation of the grains. It is emphasized that since the cavity pressures on the inclined and the parallel top facet are zero, the only way these facets can cavitate is by virtue of stress redistributions in the grains during evolution of the cavitation on the central facet. In Fig. 15(d)–(f), the normal stress distribution along the facets are plotted, again just prior to coalescence. In all three cases a compressive normal stress is found on the central facet in order to constrain cavity growth there. In Fig. 15(d), for the diffusion dominated case, the normal stress on the other facets is tensile. The magnitudes of these internal stresses are such that the separation rate is the same for all facets. In Fig. 15(f), for the larger value b_I/L_m, the normal stress distribution is strongly non-uniform in accordance with the non-uniform cavitation.

In Fig. 16(a)–(c), the development of these normal stresses in time are plotted for the centre of the facets, and in Fig. 16(d)–(f) the corresponding evolution of the separation rates $\dot{\delta}$ is normalized $R_I\dot{\varepsilon}_p$ (see Eq. (13)). The compressive stress counteracting the cavity growth on the central facet is clearly seen now to be maximal for the smaller value of b_I/L_m. Also with increasing b_I/L_m, the normal stresses keep evolving during the process; thus, the interactions evolve continually during the process. Near the end of the lifetime for the case in Fig. 16(a), the separation rates $\dot{\delta}/(R_I\dot{\varepsilon}_p)$ become very large, so that grain deformations are negligible; this demands that facets separate at the same rate, as is clearly seen in Fig. 16(d). In the case where the relative creep rate is highest, $\log(b_I/L_m) = 0.5$, it can be seen in Fig. 16(f) that the separation rates at the inclined and top facet are very small compared with that on the central facet.

The above results indicate that if $\dot{\delta}/(R_I\dot{\varepsilon}_p)$ is large, the creep deformations of the grain are negligible, so the grain will behave virtually rigidly. A consequence of this is that the separation rates of the different facets are kinematically coupled, as illustrated in Fig. 17. In this figure, the separation rate of facet i, $\dot{\delta}_i$, is coupled with the separation rate of the adjacent facet j, $\dot{\delta}_j$, according to $\dot{\delta}_j/2 = \dot{\delta}_i \sin\alpha$. In most cases where the grains behave rigidly, cavitation is dominated by diffusion and therefore controlled by the facet normal stress σ_n. Without exploring this further here, these conditions suggest a simple method of analyzing HA cavitation in large polycrystalline aggregates. Assuming uniform carbide distributions and internal pressures along each facet, but at different magnitudes (as in this section), the current (uniform) normal stress over all facets can be determined by satisfying the kinematic couplings of the separation rates. In cases where the rigid grain behaviour is present from the beginning, the time to first coalescence can be readily solved for. It seems that the kinematic coupling in case of rigid grain behaviour also holds for three-dimensional polycrystal microstructures.

6. Discussion

The results presented in Sections 4 and 5 suggest an intricate connection between the influence of variations in the cavity pressure distribution (i.e., carbide distribution) over a polycrystal and the creep resistance of the material relative to the diffusion rates. To further pin down the essential elements of this, we consider some simplifying descriptions.

The first one is a one-dimensional model consisting of two parallel bars. The idea behind this model is similar to Dyson's [20] two-bar model, which he used to demonstrate creep-constrained cavity growth during creep rupture. The two bars are imagined to represent two different parts of the material; one containing aggressive carbides and the other with less aggressive, more stable carbides, as illustrated in Fig. 18(a). The length of the bars, which must be of the order of the grain size, is taken to be $2R_I$, and in the middle of each bar we imagine a grain-boundary facet where cavitation

takes place. The main difference between bars A and B is the methane pressure inside the cavities (but also the cavity spacing or the cavity radius may differ). Both bars deform by power-law creep and the two parallel bar set may be subjected to an applied uniaxial stress Σ_2 (see Fig. 18(b)).

Due to the difference in the internal cavity pressure, cavitation at both bars will develop with different separation rates $\dot{\delta}_A$ and $\dot{\delta}_B$, respectively. In this parallel arrangement, however, both bars must elongate at the same rate. This compatibility condition reads

$$\dot{\delta}_A + 2R_I\dot{\varepsilon}_A = \dot{\delta}_B + 2R_I\dot{\varepsilon}_B, \tag{14}$$

assuming that $\delta_{A,B} \ll R_I$. Eq. Eq. (14) can be directly rewritten as

$$\frac{\dot{\delta}_A - \dot{\delta}_B}{2R_I} = \dot{\varepsilon}_B - \dot{\varepsilon}_A.$$

From this condition, it is clear that the separation rates must be equal if the grain material does not deform significantly by creep, i.e., $(\dot{\delta}_A - \dot{\delta}_B)/2R_I \gg \dot{\varepsilon}_B - \dot{\varepsilon}_A$. The separation rate $\dot{\delta}_A$ and $\dot{\delta}_B$ can only become equal by way of stress redistribution among the two bars, so as to constrain the cavity growth rate in bar A and accelerating cavitation in bar B. If the grain (bar) material deformation becomes significant, the separation rates $\dot{\delta}_A$ and $\dot{\delta}_B$ will differ and the magnitude of the (either accelerating or constraining) internal normal stress is lower. If the grain deformations are not of any significance, the normal stress redistribution will be highest and interaction is maximal.

It is of importance at this point to appreciate the role of any applied stress Σ_2. Raising the stress level will affect both the creep in the grain as well as the grain-boundary cavitation. However, the creep process is accelerated more by the applied stress Σ_2 than by the diffusional process because of the strong non-linearity in the creep relations. Hence, if cavitation is diffusion dominated and the grain (bar) material can creep deform, applying any additional stress Σ_2 will tend to decrease the interaction.

If grain deformations are significant, the magnitude of the interaction during the lifetime is not constant. The reason for this is that the separation rate $\dot{\delta}$ increases very strongly in the course of the cavity evolution (see Fig. 8(a)). As the interaction is changing continuously, there is no single simple parameter to characterize the magnitude of interaction for the whole lifetime, except in the limiting case mentioned above when grain deformations can be neglected altogether.

Although the two-bar model is illuminating in relation to the phenomena observed in Figs. 6 and 13, it cannot explain the influence of gradients of the cavity pressure distribution on the time to first coalescence, shown in the case of Fig. 12. To explain this phenomenon, we consider a second model. When there is a gradient in the separation rate $\dot{\delta}$ along the grain-boundary facet, due to variations in internal cavity pressure, as illustrated in Fig. 19(a), this gradient,

$$\dot{\gamma} = \frac{\partial\dot{\delta}}{\partial\zeta}, \tag{15}$$

has to be accommodated by shearing of the adjacent grain material, as can be seen in Fig. 19(b). The creep resistance of the grain material will induce a normal stress distribution on the facet, as shown schematically in Fig. 19(c). These stresses will also tend to constrain rapid cavitation (i.e. large $\dot{\delta}$) and accelerate slow growth (i.e., small $\dot{\delta}$). Here, also, if the grain cannot deform significantly, severe stress redistributions have to take place to make the $\delta(\zeta)$ and $\dot{\delta}(\zeta)$ uniform. With this simple model, it can be understood how a larger gradient in cavity pressure distribution gives rise to a larger gradient in $\dot{\delta}$ which will result in higher interaction stresses that constrain cavity growth from aggressive carbides more, giving a more uniform cavitation.

A rough indication about whether or not cavitation will be uniform can be obtained by comparing the separation rate $\dot{\delta}$ with the creep deformability of the grain expressed in $\dot{\varepsilon}_g$. This leads to the dimensionless number $(\dot{\delta}/l)/\dot{\varepsilon}_g$, where l is the distance over which interaction is investigated. For example in Section 4, the l can be taken as the wavelength of the pressure distribution or as the facet width R_I, while $\dot{\varepsilon}_g$ can be identified as $\dot{\varepsilon}_p$ defined in Eq. (13). Then, as we have seen in the previous Sections (e.g., Figs. 8, 10 and 16), interaction is strong (cavitation is uniform) when $\log(\dot{\delta}/l)/\dot{\varepsilon}_g$ is roughly larger than 1, whereas interaction is negligible when $\log(\dot{\delta}/l)/\dot{\varepsilon}_g < -1$ or so. When the wavelength of the pressure distributions decreases, $(\dot{\delta}/l)/\dot{\varepsilon}_g$ increases and therefore the interaction increases, as we have found in Section 4. When subjected to applied stresses Σ_1 and Σ_2 (see Fig. 1), we take as a rough measure of the creep deformability of the grain

$$\dot{\varepsilon}_g = \dot{\varepsilon}_0(\bar{p}_m + \Sigma_e)/\sigma_0)^n,$$

incorporating creep due to both internal cavity pressure and external stress. For the separation rate $\dot{\delta}$, only the contribution of diffusion is taken into account (in situations where creep controls cavity growth, the creep rate in the grains is so high that $\dot{\varepsilon}_g$ dominates anyway). Then with Eq. (9) and neglecting the creep term in Eq. (11), the separation rate is found as

$$\dot{\delta} = 4\frac{\mathscr{D}}{b^2}\frac{\bar{p}_m + \Sigma_2}{d(f)},$$

where $d(f) = \ln(1/f) - (3-f)(1-f)/2$. Only if $f \ll 1$ is $d(f)$ large, but during most of the lifetime, $d(f)$ is of the order of 1. When non-uniformity on the grain-size scale is investigated, l should be taken as R_I. Substituting this, one obtains

$$\frac{\dot{\delta}}{l\dot{\varepsilon}_g} \approx 4\frac{b}{R_I}\left(\frac{L_g}{b}\right)^3, \quad \text{where } L_g^3 = \frac{\mathscr{D}(\bar{p}_m + \Sigma_2)}{\dot{\varepsilon}_0((\bar{p}_m + \Sigma_e)/\sigma_0)^n} \tag{16}$$

The term L_g/b in the right-hand side is the most important parameter since it relates the creep deformability of the grains to the diffusion parameter of the grain-boundary cavitation. When L_g/b is very large, grain deformation is not expected to become significant so that cavitation is expected to be uniform. When b/L_g is very large, cavitation will be non-uniform. A grain size effect enters through the ratio b/R_I.

7. Conclusion

Real materials always contain different types of carbides, which leads to different equilibrium methane pressures. In general, the time to first cavity coalescence by HA is affected by the volume fractions of different carbides and their distributions inside the material. The main conclusion from the present study is that growth of all cavities is coupled in general by creep, by virtue of mechanisms similar to those first proposed by Dyson [9]. This leads to internal stresses that tend to constrain cavity growth in areas with above-average methane pressures resulting from relatively unstable carbides present there. Evidently, the HA resistance of a material is enhanced by reducing the amount of unstable carbides; but this study shows that the lifetime does not simply scale with the amount of unstable carbides.

Unfortunately, a simple accurate estimate of the time to failure does not seem to be feasible in general. However, there are two limiting cases: (i) creep is so fast that creep constraints disappear; (ii) diffusion is so fast that constraint enforces uniform growth of all cavities irrespective of their internal pressure. In the first case, cavity evolution can be determined directly from cavity growth relations, Eqs. (5)–(10), by substituting the applied stresses. The second case allows for an estimate assuming rigid grains. A rough estimate whether or not the current HA conditions are a limiting case can be obtained through the value of the parameter defined in Eq. (16).

Acknowledgements

The research of Marc van der Burg is sponsored by the Shell Research and Technology Center, Amsterdam, The Netherlands.

References

[1] *American Petroleum Institute Publication 941*, 4th edn., 1990.
[2] M.W.D. van der Burg, E. van der Giessen and R.C. Brouwer, *Acta Mater.*, *44* (1996) 505.
[3] H.-M. Shih and H.H. Johnson, *Acta Metall.*, *30* (1982) 537.
[4] T.A. Parthasarathy, *Acta Metall.*, *33* (1985) 1673.
[5] P.G. Shewmon, *Acta Metall.*, *35* (1987) 1317.
[6] A. Needleman and J.R. Rice, *Acta Metall.*, *28* (1980) 1315.
[7] T.-L. Sham and A. Needleman, *Acta Metall.*, *31* (1983) 919.
[8] E. van der Giessen, M.W.D. van der Burg, A. Needleman and V. Tvergaard, *J. Mech. Phys. Solids*, *43* (1995) 123.
[9] B.F. Dyson, *Met. Sci.*, *10* (1976) 349.
[10] V. Tvergaard, *J. Mech. Phys. Solids*, *32* (1984) 373.
[11] E. van der Giessen and V. Tvergaard, *Acta Metall. Mater.*, *42* (1994) 959.
[12] M.W.D. van der Burg and E. van der Giessen, in S.I. Andersen et al. (eds.), *15th Risø Int. Symp. Materials Science 1994*, Risø National Laboratory, Roskilde, Denmark, 1994, p. 263.
[13] M.W.D. van der Burg and E. van der Giessen, in A.W. Thompson and N.R. Moody (eds.), *5th Int. Conf. the Effects of Hydrogen on Material Behavior, Moran, Wyoming, 1994*, TMS, Warrendale, PA, 1994, p. 313.
[14] G.R. Odette and S.S. Vagarali, *Metall. Trans. A*, *13* (1982) 299.
[15] T.A. Parthasarathy and P.G. Shewmon, *Metall. Trans. A*, *15* (1984) 2021.
[16] P.G. Shewmon, *Mater. Sci. Technol.*, *1* (1985) 1.
[17] D. Hull and D.E. Rimmer, *Philos. Mag.*, *4* (1959) 673.
[18] A.C.F. Cocks and M.F. Ashby, *Progr. Mater. Sci.*, *27* (1982) 199.
[19] E. van der Giessen and V. Tvergaard, *Mech. Mater.*, *17* (1994) 47.
[20] B.F. Dyson, *Rev. Phys. Appl.*, *23* (1988) 605.